Bioinspir. Biomim. **8** (2013) 036002 (16pp) doi:10.1088/1748-3182/8/3/036002

Robust hopping based on virtual pendulum posture control

Maziar A Sharbafi[1,2], Christophe Maufroy[2], Majid Nili Ahmadabadi[1], Mohammad J Yazdanpanah[1] and Andre Seyfarth[2]

[1] School of ECE, Control and Intelligent Processing Center of Excellence (CIPCE), College of Engineering, University of Tehran, Tehran, Iran
[2] Lauflabor Locomotion Laboratory, Technical University of Darmstadt, Darmstadt, Germany

E-mail: sharbafi@ut.ac.ir

Received 29 October 2012
Accepted for publication 14 May 2013
Published 5 June 2013
Online at stacks.iop.org/BB/8/036002

Abstract
A new control approach to achieve robust hopping against perturbations in the sagittal plane is presented in this paper. In perturbed hopping, vertical body alignment has a significant role for stability. Our approach is based on the virtual pendulum concept, recently proposed, based on experimental findings in human and animal locomotion. In this concept, the ground reaction forces are pointed to a virtual support point, named virtual pivot point (VPP), during motion. This concept is employed in designing the controller to balance the trunk during the stance phase. New strategies for leg angle and length adjustment besides the virtual pendulum posture control are proposed as a unified controller. This method is investigated by applying it on an extension of the spring loaded inverted pendulum (SLIP) model. Trunk, leg mass and damping are added to the SLIP model in order to make the model more realistic. The stability is analyzed by Poincaré map analysis. With fixed VPP position, stability, disturbance rejection and moderate robustness are achieved, but with a low convergence speed. To improve the performance and attain higher robustness, an event-based control of the VPP position is introduced, using feedback of the system states at apexes. Discrete linear quartic regulator is used to design the feedback controller. Considerable enhancements with respect to stability, convergence speed and robustness against perturbations and parameter changes are achieved.

(Some figures may appear in colour only in the online journal)

List of symbols, terms and definitions

Nomenclature

CoM	Center of mass
GRF	Ground reaction force
VBLA	Velocity-based leg adjustment
TD	Touch down
TO	Take off
MLC	Maximum leg compression
VPP	Virtual pivot point
VP	Virtual pendulum
VPPC	VP posture control
LQR	Linear quadratic regulator
VPPC-FP	VPPC with fixed point
VPPC-LQR	VPPC with LQR
aVPPC	Approximate VPPC
eVPPC	Exact VPPC
SLIP	Spring loaded inverted pendulum
TSLIP	SLIP extended by trunk
XTSLIP	eXtended TSLIP

Model parameters

m_t	Trunk mass (kg)
m_l	Leg mass (kg)
m	Total mass (kg)
J_t	Trunk moment of inertia (kg m^2)
J_l	Leg moment of inertia (kg m^2)
r_{CoM}	Distance hip to trunk CoM (m)

r_{leg}	Distance hip to leg CoM (m)
l_0	Leg rest length (m)
g	Gravitational acceleration (m s^{-2})
k	Dimensionless leg stiffness
$\tilde{d}$	Dimensionless leg damping
r_{VPP}	Distance VPP to trunk CoM (m)
γ	VPP angle (deg)
μ	Leg adjustment parameter
F_{leg}	Leg force (N)
y_d	Desired hopping height (m)

States for TSLIP

x	Horizontal position of CoM
y	Vertical position of CoM
φ	Trunk angle

States for XTSLIP

x	Horizontal position of hip
y	Vertical position of CoM
φ_l	Leg angle
φ	Trunk angle

1. Introduction

The ability to perform efficient and robust locomotion is a crucial condition for the more extensive use of legged robots in real world applications. In that respect, robots can learn from animals, if the principles underlying locomotion in biological legged systems can be transferred to their artificial counterparts. A great progress in this direction was introducing simple models, coined 'templates' [1], able to represent the overall dynamics of animal gaits. One of the most famous models is spring-loaded inverted pendulum (SLIP) [2, 3] which consists of a point mass atop a massless spring and provides a good description of human gaits, such as walking [4], hopping and running [2]. Despite its high level of abstraction, it supported and inspired the development of successful legged robots [5, 6] or was used as explicit targets for control [7], over the years.

In this model, leg force is assumed to be proportional to the amount of leg compression, i.e. the shortening of the leg length measured between center of mass (CoM) and the contacting point at the ground. At the same time, this model assumes that leg forces are directed towards the CoM. However, experimental data indicate that measured leg forces do not point exactly to the CoM but sometimes intersect at a point above it, called virtual pivot point (VPP) [8] or divergent point (DP) [9]. In order to represent this observation in the model, the SLIP must be extended to include a model of the upper body. It is modeled by the addition of a rigid trunk to SLIP which will be called hereafter as TSLIP (for trunk-SLIP). Then, hip torques can be calculated to deviate forces generated by the leg spring to intersect at the VPP and the stabilization of the upright posture (or *posture control*) can be achieved. In this model, the hip torque depends on the amount of the leg force and the angular orientation of the leg with respect to the trunk. Most of the control methods rely on the feedback control of the trunk orientation with respect to an absolute referential frame [5, 7, 10]. In contrast, this VPP-based control scheme was shown to be capable of supporting upright trunk posture during locomotion without the need to explicitly measure the trunk orientation with respect to the gravity direction. Similar to the adjustment of leg parameters (e.g. leg stiffness/rest length) in the SLIP model, the position of the VPP can be considered as a control target. This approach was validated in simulations, where it yielded stable upright walking and running patterns [11].

In this paper, we apply this concept to achieve a robust hopping, considered as running with zero forward velocity. Hopping offers the most fundamental framework to investigate the structure of such a controller. Although it may appear as a simple gait, during hopping the leg angle must be adjusted during the flight phase to achieve stable motion. This is not the case for running, for which simply placing the leg at a fixed angle with the ground is sufficient for achieving stability [12]. Hence, we have to introduce a control layer adjusting the leg angle during the swing phase which was not considered in former studies dealing with VP-based control [11, 8]. The preliminary results of this approach on the TSLIP model are presented in our previous work [13]. Since the presented controller is not able to control the hopping height, another controller is required for energy management. Leg rest length adjustment during the stance phase is presented to solve this problem as the third control layer.

As the simulation models predict already asymptotically stable gait patterns with a fixed VPP location [8], step-to-step changes in VPP placement could further enhance gait stability and robustness. This can speed up the slow convergence to a steady state and increase the robustness against perturbations. Previous investigations also showed that placing the VPP out of the trunk axis could be used for maneuver [11] or compensation of energy losses [14]. In this study, we use a similar approach to solve the issues regarding disturbance rejection and robustness. With the VP concept, the complex process of generating a suitable hip torque pattern is simplified to the specification of the position of one point. Hence, it is particularly suited for the application of event-based control. It is performed by a feedback law using the states at the apex event in order to adjust the VPP position during the next stance phase. In order to approach real robot characteristics, mass and damping are added to the leg to verify the control approach capabilities under more realistic conditions. These extensions of the model introduce new challenges in different control layers during the flight and stance phases.

2. Methods

2.1. Models

Our models extend the SLIP [2, 3], a template [1] widely used to describe bouncing gaits in animals [15], and are implemented to various extents in many legged robots [5, 7, 16–19]. Two extensions are considered here that include important features present in real robotic systems but missing in the traditional SLIP model. To ensure realistic properties, we use as much as possible parameters derived from the human case.

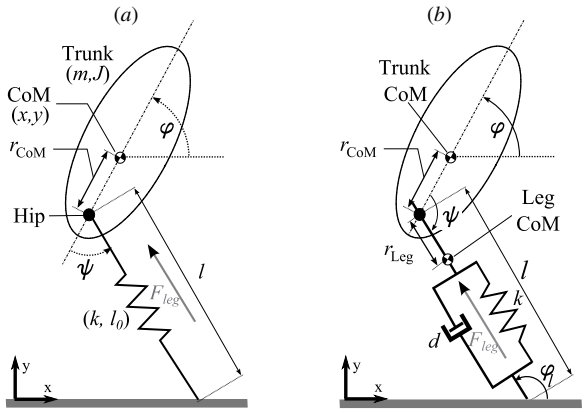

Figure 1. (*a*) TSLIP model with a rigid trunk and a massless prismatic spring for the leg. (*b*) XTSLIP model with the mass, spring and damper in the leg.

Table 1. Model fixed parameters for human [21].

Parameters	Symbol	Value (units) TSLIP	XTSLIP
Trunk mass	m_t	80 (kg)	54 (kg)
Leg mass	m_l	–	26 (kg)
Trunk moment of inertia	J_t	10.5 (kg m^2)	10.6 (kg m^2)
Leg moment of inertia	J_l	–	2.76 (kg m^2)
Distance hip to trunk CoM	r_{CoM}	0.075 (m)	0.33 (m)
Distance hip to leg CoM	r_{leg}	–	0.45 (m)
Leg rest length	l_0	1 (m)	1 (m)
Gravitational acceleration	g	9.81 (m s^{-2})	9.81 (m s^{-2})

2.1.1. TSLIP model. The first extension consists in replacing the point mass by an extended trunk, as represented in figure 1(*a*). In our simulations, the model parameters (table 1) are set to match the characteristics of a human with 80 kg weight and 1.89 m height. In the TSLIP[3], all the body mass is considered to be concentrated in the trunk.

When the leg does not touch the ground, the CoM moves in a ballistic motion named the flight phase, where the leg orientation can be arbitrarily adjusted (as the leg is massless). The stance phase starts when the distal end of the leg hits the ground (this event is called TD for touchdown) and ends when the vertical component of the ground reaction force (GRF) is equal to zero (this event is called TO for takeoff). During the stance phase, the spring force, the hip torque and the gravity affect the motion. Using l, l_0 and k for the current leg length, the leg rest length and the spring stiffness, respectively, the leg force F_{leg} is generated by the spring along the leg axis given by $F_s = k\ (l_0 - l)$ (see figure 1(*a*)). A torque can be applied at the hip to stabilize the posture of the trunk. Symbols x, y and φ are used to represent the CoM horizontal and vertical positions and the trunk orientation, respectively.

2.1.2. XTSLIP model. In the second step, additional features are introduced to reach a more realistic model of the leg. We refer to this model as XTSLIP, for eXtended-TSLIP (eTSLIP).

[3] In [20], a similar model was introduced, namely ASLIP, for 'asymmetric SLIP'. However, as this term can also designate an SLIP model with asymmetric leg properties, we prefer to use the name TSLIP.

First, part of the total mass is transferred from the trunk to the leg, as shown in figure 1(*b*). The total mass is divided between the leg and the trunk in a human-like proportion, as given in table 1. One consequence is that an impact with the ground occurs at TD. It is modeled to be instantaneous and completely inelastic. Concretely, an impulse is applied at the foot tip that brings its velocity to zero. We consider that only the part of the leg placed above the spring has significant mass. Hence, the impact along the leg axis is neglected and the impulse acts perpendicular to the leg axis. Another consequence of the addition of the leg mass is that hip torque is also required during the flight phase to adjust the leg angle. This causes a perturbation of the trunk orientation during the flight phase that must be handled by the controller during the stance phase.

Second, damping in the leg spring is introduced with a coefficient d producing a resistant force $F_d = -\mathrm{d}\dot{l}$. The leg force is then given by $F_{\text{leg}} = F_s + F_d$ (see figure 1(*b*)). For convenience, we define the dimensionless leg stiffness $\tilde{k} = kl_0/mg$ and damping ratio $\tilde{d} = \frac{d}{2\sqrt{mk}}$ which are used hereafter instead of k and d.

The leg orientation, that must be introduced to characterize the system state, is denoted φ_l, while x, y and φ are used here for hip point horizontal and vertical positions and trunk orientation. Details of the system equation derivation are presented in appendix A.

2.2. Overview of the control system

Similar to the approach followed in the pioneer work of Raibert [5], we decompose the hopping control problem into three separated tasks: (*a*) upright posture, (*b*) forward speed and (*c*) hopping height controls (see figure 2). Upright posture (*a*) and hopping height (*c*) controls are active during the stance phase, while forward speed control (*b*) is active during the flight phase. The main focus of this paper is on upright posture control, which is performed with a new approach based on the VP concept. This part of the controller is explained in detail in section 2.3. The strategies for the two other control tasks are only briefly presented in section 2.4

2.2.1. Events used for control purpose. Four events are defined for control purposes. Two of them, the TD and TO, were already defined in section 2.1.1. They are used to switch between the control tasks during the swing and stance phases, respectively. Additionally, two other events are defined: apex and maximum leg compression (MLC). Apex is the instant during the flight phase where the system reaches its maximum altitude. Hence, it is characterized by $\dot{y} = 0$ with $\ddot{y} < 0$. On the other hand, MLC is the instant during the stance phase where the leg reaches its minimum length, i.e. $\dot{l} = 0$ with $\ddot{l} > 0$.

2.2.2. Periodic hopping motions and stability analysis. Stability of the hopping motion is investigated using Poincaré return map analysis, with the apex as the event to define the Poincaré section. It is based on the definition of the mapping function **F**, called the Poincaré return map, relating

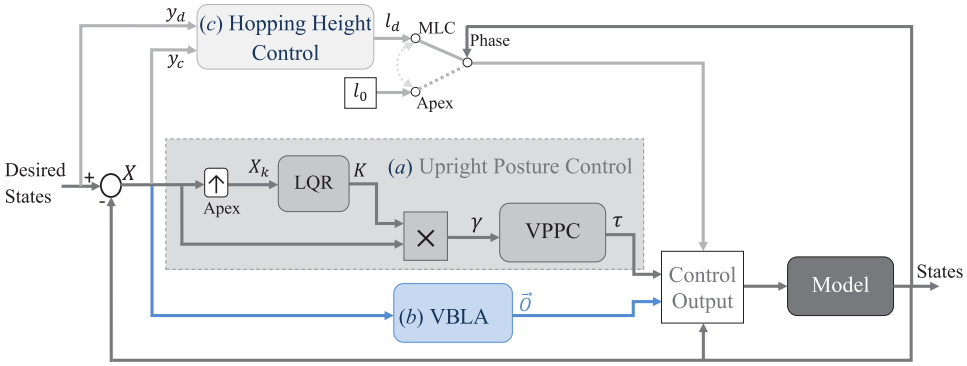

Figure 2. Illustration of our three-layered controller, which includes: (*a*) upright posture control using VPPC with event-based control at apex. This module gives hip torque τ during stance. (*b*) Forward speed control using the velocity-based leg adjustment (VBLA) during flight phase. $\vec{O}$ is the vector showing the leg direction. (*c*) Hopping height control gives desired rest length l_d at maximum leg compression (MLC) moment. Leg rest length adjustment put l_0 and l_d at apex and MLC, respectively.

the state $\mathbf{S}$ of the system at the crossing of two successive sections, denoted as k and $k+1$. This relation can be written as $\mathbf{S}_{k+1} = \mathbf{F}(\mathbf{S}_k)$. First, fixed points $\mathbf{S}^*$ of $\mathbf{F}$, defined by $\mathbf{S}^* = \mathbf{F}(\mathbf{S}^*)$, have to be identified. These correspond to the periodic motions of the system. In our case, the dimension of the state vector to be considered for the Poincaré return map analysis can be reduced. According to the definition of apex, $\dot{y}$ is always equal to zero and can be omitted. For steady locomotion, the horizontal position x and its periodicity are considered irrelevant (but of course not the forward velocity $\dot{x}$) and is also omitted. Moreover, for upright hopping on place, fixed points can be found *a priori*, as $\dot{x}$ must be equal to 0, the angles (φ and φ_l) equal to 90° and the angular velocities ($\dot{\varphi}$ and $\dot{\varphi}_l$) equal to 0. Hence, each fixed point is simply characterized by its nominal hopping height, denoted here by y^*. Accordingly, the state vector $\mathbf{S}$ of the system at apex and the fixed points $\mathbf{S}^*$ are

$$\mathbf{S} = \begin{cases} [y, \varphi, \dot{x}, \dot{\varphi}] & \text{for TSLIP} \\ [y, \varphi_l, \varphi, \dot{x}, \dot{\varphi}_l, \dot{\varphi}] & \text{for XTSLIP;} \end{cases}$$
$$\mathbf{S}^* = \begin{cases} [y^*, 90^\circ, 0, 0] & \text{for TSLIP} \\ [y^*, 90^\circ, 90^\circ, 0, 0, 0] & \text{for XTSLIP.} \end{cases} \quad (1)$$

Next, the local stability of the fixed points must be investigated by computing the eigenvalues λ_j of the Jacobian matrix $A = \frac{\partial \mathbf{F}}{\partial \mathbf{S}}(\mathbf{S}^*)$ (in our case, A is evaluated numerically). If the largest eigenvalue (with the maximum magnitude) has an amount smaller than (or equal to) 1, then the periodic solution is asymptotically stable (or partially stable). Then, defining $\lambda_{\text{Max}} = \max_j |\lambda_j|$, the asymptotically stability condition will be $\lambda_{\text{Max}} < 1$.

2.3. Virtual pendulum posture control

2.3.1. Virtual pendulum concept for postural stabilization. The key idea of the VP concept is to create a point of virtual support (virtual pivot point or VPP) located above the CoM by redirecting the GRF vector towards this point, at each instant of the stance phase. Hence, the trunk behavior is transformed, from an inverted pendulum mounted at the hip to a regular

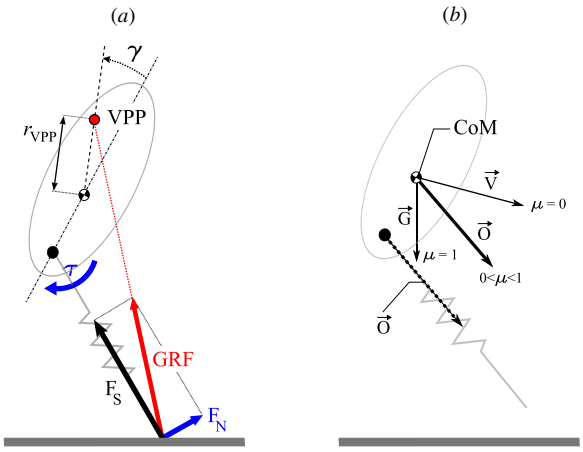

Figure 3. (*a*) Virtual pendulum-based posture control (VPPC) during the stance phase. (*b*) Velocity-based leg adjustment (VBLA) during the flight phase.

VP suspended at the VPP (see [8] for details). In simulation, the redirection of the GRF vector is achieved by applying a torque (τ) at the hip during the stance phase (figure 1(*a*)), hence generating a force perpendicular to the leg axis (F_N). We call this approach *virtual pendulum-based posture control* or VPPC. For the TSLIP model, as the leg is massless, this torque is easily computed as

$$\tau = F_S\, l\, \frac{r_{\text{CoM}}\ \sin\ \psi + r_{\text{VPP}}\ \sin(\psi - \gamma)}{l + r_{\text{CoM}}\ \cos\ \psi + r_{\text{VPP}}\ \cos(\psi - \gamma)}, \quad (2)$$

where r_{CoM} and r_{VPP} are the distance of the CoM to hip and VPP, respectively, and γ is the angle between VPP and the trunk orientation (see figure 3(*a*)). Careful examination of equation (2) reveals that the computation of τ does not require information about the absolute trunk orientation φ. Only the force F_S and the leg orientation w.r.t. the body ψ are needed.

For the XTSLIP model, the application of a torque to the leg at the hip does not only translate in a force perpendicular to the leg axis, but can also result in the acceleration of the leg with mass. As a result, the expression of τ to redirect the GRF exactly towards the VPP is more complex than equation (2). Its derivation is presented in appendix B. The

computation of τ now generally requires the knowledge of the full system states, including the absolute trunk orientation φ. Hence, the strict application of the VPPC to the XTSLIP model drastically increases the requirements with respect to sensory information. For this reason, we considered two implementations of the VPPC for the XTSLIP model.

- *aVVPC* or approximate-VPPC, using the simple equation (2).
- *eVPPC* or exact-VPPC, using the exact expression of τ given by equation (B.2) in appendix B.

Besides the redirection of the GRF towards the VPP, another aspect of the VPPC is the choice of the VPP position and its possible adjustment from step to step. Regarding this latter aspect, we investigated in this paper two approaches, presented in the following sections.

2.3.2. VPPC with fixed VPP position (VPPC-FP). This is the simplest case, where the position of the VPP is fixed with respect to the frame attached to the trunk. To result in an upright posture of the trunk during steady state hopping, the VP concept indicates that the VPP must lie on the trunk axis, or equivalently $\gamma = 0$. Hence, only r_{VPP} is used to characterize the VPP position.

2.3.3. VPPC with event-based control (VPPC-LQR). In this case, the VPP position is adapted once per period using event-based control, leading to the improvement of the performance and robustness of the hopping motion. At each apex, the new VPP position is computed for the next stance phase using the current system state. As it will become clear later, this computation is based on discrete linear quartic regulator (LQR). Hence, this approach is named here VPPC-LQR.

To design the controller, the Poincaré return map is first linearized around a nominal fixed point S^*. Note that the map generally depends on the model parameters and the control parameters, including the position of the VPP for VPPC as well as the parameters for the other control tasks. Here, the latter are taken constant and only the variables parameterizing the VPP position, i.e. r_{VPP} and γ, are considered as inputs (index k denotes the variables in the k^{th} apex):

$$\Delta\mathbf{S}_{k+1} = \mathcal{A}_S\,\Delta\mathbf{S}_k + \mathcal{B}_\gamma\,(\gamma_k - \gamma^*) + \mathcal{B}_r\,(r_{\mathrm{VPP}} - r^*_{\mathrm{VPP}}), \quad (3)$$

with

$$\Delta\mathbf{S}_k = \mathbf{S}_k - \mathbf{S}^* = \begin{cases} [\Delta y_k, \Delta\varphi_k, \Delta\dot{x}_k, \Delta\dot{\varphi}_k] & \text{for TSLIP} \\ [\Delta y_k, \Delta\varphi_{lk}, \Delta\varphi_k, \Delta\dot{x}_k, \Delta\dot{\varphi}_{lk}, \Delta\dot{\varphi}_k] & \text{for XTSLIP} \end{cases} \quad (4)$$

$$\mathcal{A}_S = \frac{\partial\mathbf{F}}{\partial\mathbf{S}}(\mathbf{S}^*, \gamma^*, r^*_{\mathrm{VPP}}) \quad (5)$$

$$\mathcal{B}_\gamma = \frac{\partial\mathbf{F}}{\partial\gamma}(\mathbf{S}^*, \gamma^*, r^*_{\mathrm{VPP}}); \quad \mathcal{B}_r = \frac{\partial\mathbf{F}}{\partial r_{\mathrm{VPP}}}(\mathbf{S}^*, \gamma^*, r^*_{\mathrm{VPP}}). \quad (6)$$

Following the same argument as for the VPPC with fixed VPP position, the nominal VPP angle γ^* must be equal to 0. Additionally, the vector $\mathcal{B}_r$ is also equal to 0. Indeed, varying r_{VPP} has no effect on the motion when the trunk is exactly vertical, which is the case of the periodic motion corresponding to the fixed point. The remaining matrices $\mathcal{A}_S$ and $\mathcal{B}_\gamma$ have the following form:

$$\mathcal{A}_S = \begin{pmatrix} \lambda & 0 \\ 0 & A \end{pmatrix}; \qquad \mathcal{B}_\gamma = \begin{pmatrix} 0 \\ B \end{pmatrix} \quad (7)$$

in which λ is the eigenvalue of the vertical position dynamics, and A and B are respectively $[n \times n]$ and $[n \times 1]$ matrices, where $n = 3$ and $n = 5$ for TSLIP and XTSLIP, respectively. This indicates that the dynamical model can be decoupled in the vertical position y, which is not controllable using γ_k, and the rest states. Defining

$$\mathbf{X}_k = \begin{cases} [\Delta\varphi_k, \Delta\dot{x}_k, \Delta\dot{\varphi}_k] & \text{for TSLIP} \\ [\Delta\varphi_{lk}, \Delta\varphi_k, \Delta\dot{x}_k, \Delta\dot{\varphi}_{lk}, \Delta\dot{\varphi}_k] & \text{for XTSLIP} \end{cases} \quad (8)$$

we can rewrite the linear system as

$$\begin{cases} \Delta y_{k+1} = \lambda\Delta y_k \\ \mathbf{X}_{k+1} = A\,\mathbf{X}_k + B\,\gamma_k. \end{cases} \quad (9)$$

Using hopping height control, we can stabilize the first part of the system by ensuring that λ is smaller than 1 (as described in section 2.4.2). If the pair (A, B) is controllable, then the evolution of $\mathbf{X}_k$ can also be controlled by using a linear state feedback law for γ_k:

$$\gamma_k = -K\,\mathbf{X}_k. \quad (10)$$

The coefficients of K can be chosen to place the poles of the resulting close loop system matrix $A - BK$ in desired positions.

In our previous work [13], two methods to select the coefficients of K were investigated for the TSLIP model, without hopping height control. We present here only the more advantageous method, based on optimal feedback control. This approach allows a smooth convergence of the state variables to their steady state values. Representing the input γ at the kth apex with $\mathbf{u}_k$, we use discrete LQR [22] with a cost function J shown in equation (11). The importance of the states and the input are determined by positive definite (here diagonal) matrix Q and scalar R when there exists only one input. In discrete LQR, R could be even equal to zero; then, the only control target will be minimizing the states that should converge to zero:

$$J = \sum_{k=1}^{\infty} \mathbf{X}_k^T Q\mathbf{X}_k + \mathbf{u}_k^T R\mathbf{u}_k \overset{R=0}{\Longrightarrow} J = ||W\mathbf{X}||_2^2, \quad (11)$$

where W is a diagonal weight matrix and $Q = W^TW$. Without R, the gain vector K is given by equation (12), in which P is a the solution of the discrete Riccati algebraic equation (13). With a symmetric matrix for Q as defined before, P will be a symmetric positive definite matrix:

$$K = (B^TPB)^{-1}B^TPA \quad (12)$$

$$P = Q + A^T(P - PB(B^TPB)^{-1}B^TP)A. \quad (13)$$

The weight matrix W can be used to give more importance to the behavior of some of state variables.

2.4. Leg adjustment

2.4.1. Leg adjustment during the swing phase (VBLA). Unlike running [12] and walking [4], stable hopping cannot be achieved with a fixed angle of attack with respect to the ground. It means that finding an appropriate leg angle adjustment during the flight phase is needed for hopping in place. Most leg adjustment strategies rely on sensory information about the CoM velocity, following the Raibert approach [5] in which the foot landing position is adjusted based on the horizontal velocity (for example [23] and [7]). Recently, various strategies were investigated by Peuker *et al* [24] who concluded that leg placement with respect to both the CoM velocity and the gravity vectors yielded the most robust and stable hopping and running motions with the SLIP model. In this paper, a modified version of this strategy is used: the leg direction is given by vector $\vec{O}$, a weighted average of the CoM velocity vector $\vec{V}$ and the gravity vector $\vec{G}$. The weight of each vector is determined by coefficient $0 < \mu < 1$ (see figure 1(*b*)):

$$\vec{V} = [v_x, v_y]^T; \qquad \vec{G} = [0, -g]^T$$
$$\vec{O} = (1-\mu)\vec{V} + \mu\vec{G}. \tag{14}$$

When $\mu = 0$, the leg is parallel to the CoM velocity vector and, for $\mu = 1$, the leg is exactly vertical. In [24], only the direction of the velocity vector was considered. Using its magnitude as well, the robustness of the method against high perturbations is increased. In the rest of the paper, we will refer to this strategy as the velocity-based leg adjustment or VBLA.

In TSLIP, no hip torque during the flight phase is needed to set the leg angle. With the addition of leg mass in XTSLIP, a position controller for leg angle is required at the hip joint. In order to track the desired leg direction, a PD controller ($\tau = k_p(\phi_l - \phi_l^d) + k_d\dot{\phi}_l$, with ϕ_l^d for desired leg angle) is applied to set the hip torque. In addition, to prevent high hip torques, we employed saturation with maximum torque 400 Nm (200 Nm for each leg)[4]. Although it permits desirable tracking, the trunk angle will change which should be compensated in the next stance phase.

2.4.2. Hopping height control. As discussed in section 2.3.3, with linearizing the system dynamics around the fixed point, the vertical position dynamics can be decoupled. The goal of the hopping height control is to stabilize this dynamics, i.e. to ensure that the absolute value of λ in equation (9) is smaller than 1. There exist different strategies in hopping height control using leg rest length and stiffness adjustment like [27, 28] and [29]. Since changing the leg rest length is easier to implement on robots, we introduce a simple method to adjust the leg rest length once in each stance phase (and returning to nominal value at each apex). This also avoids using time-based (open loop) techniques [27] or complex solutions which needs many measurements and actuations [29].

[4] Typical hip torque values for human running and one leg hopping are less than 150 and 60 Nm, respectively [25] and [26]. In perturbed hopping, more torque is needed to remove the perturbation and for zeroing the velocity.

Assuming the spring-mass model for hopping, the vertical dynamics for the flight and swing phases of motion are given in

$$\begin{cases} \ddot{y} = -g & \text{during flight phase} \\ m\ddot{y} = -mg + k(l_0 - y) - d\dot{y} & \text{during stance phase.} \end{cases} \tag{15}$$

The preferred hopping height in humans [30] is 5 cm. The desired hopping height (y_d) is the desired height of body CoM at apex. Thus, in order to achieve hopping like humans, this value is set to 1.125 m according to table 1. The target is to balance the energy to bring back the body CoM to y_d at the next apex. This may be performed by injecting or absorbing energy regarding the energy of the system and losses. In this method, the leg rest length is changed to a new value (l_d) at MLC, based on the value of the leg length at this instant (noted y_c) and the required TO vertical velocity V_{to} to reach y_d.

For vertical hopping, it is possible to do it in only one step that means $\lambda = 0$, which equivalently realizes dead beat hopping height control. The leg rest length returns to its initial length (l_0) at the next apex. Solving the differential equation of the stance phase and using the relation between V_{to}, l_d and y_d result in the following equations that should be solved numerically (for details see appendix C):

$$l_d = y_c + \frac{mg}{k} - a\sqrt{\frac{1+P_{l_d}^2}{1+\beta^2}}\exp(\beta(\gamma - \arctan(P_{l_d})) \tag{16}$$

$$P_{l_d} = \beta + \frac{\overbrace{s + \sqrt{s^2 + 2g(y_d - l_d)}}^{v_{to}}}{a\omega} \tag{17}$$

in which, $s = \frac{dg}{k}$, $a = \frac{mg - dv_{to}}{k}$, $\beta = \frac{d}{2m\omega}$, $\gamma = \arcsin\left(\frac{\beta}{\sqrt{1+\beta^2}}\right)$ and $\omega = \sqrt{\frac{4\,\text{km} - d^2}{4m^2}}$ is the stance motion frequency. Of course, if $d^2 \geqslant 4$ km, the damping is too high to achieve a periodic motion.

2.5. Evaluation of the controller

The effectiveness of the controller is evaluated with respect to the following criteria: stability and robustness. As mentioned in section 2.2.2, the stability of a periodic hopping motion is evaluated using the eigenvalues of the linearized Poincaré map around the corresponding fixed point. Asymptotic stability requires all eigenvalues to be placed inside the unit circle. The magnitude of the largest eigenvalue $\lambda_{\max}$ can also be used to characterize the disturbance rejection rate in the vicinity of the limit cycle, with smaller values being the indicator of faster disturbance rejection. In addition, the disturbance rejection ability provided by the different controllers is illustrated by the transient behavior of the system after the application of a perturbation of the horizontal velocity $\dot{x}$, the trunk angle φ and/or angular velocity $\dot{\varphi}$ to the model.

For stable hopping, the robustness is evaluated by quantifying the largest perturbation from which the system can recover. For this purpose, perturbations of $\dot{x}$, φ and $\dot{\varphi}$ are considered separately. In order to assess the level of stability (i.e. the convergence to the fixed point after perturbation

occurrence), we define a neighborhood area for the fixed point. In our experiment with six subjects performing vertical hopping, the segment kinematics were measured by markers placed on representative body landmarks using a high-speed infrared motion capture system (Qualisys with sampling rate 250 Hz). The standard deviation of the horizontal velocity, the hopping height, the trunk angle and angular velocity at apex are 3.7 cm s^{-1}, 1.5 cm, 1.16 deg and 6 deg s^{-1}, respectively. Since our hopping height control is dead beat, a very small range for apex height is selected. For the remaining parameters, we define the neighborhood area with ranges about 1.5 times of the standard deviations in human hopping as $A_n := \{\mathbf{X} | \dot{x} < 5\,\text{cm}\,\text{s}^{-1}, y - y^* < 0.5\,\text{cm}, \varphi - 90 < 2\,\text{deg}, \dot{\varphi} < 10\,\text{deg}\,\text{s}^{-1}\}$. For defining the robustness, a subset of the neighborhood area is selected regarding the type of the perturbation. To quantify the stability of each trial, a 100-step convergence condition for a specific perturbation is introduced.

Definition 1. *100-step convergence condition: a controller satisfies the neighborhood condition for a specific initial conditions set ($IC = [\dot{x}_0, \varphi_0, \dot{\varphi}_0]$), if it can move all the states to the neighborhood area at most in 100 steps and keep them there afterward.*

The tolerable amounts for evaluating the robustness of controller (C) are computed as follows.

- $\Delta\dot{x}_{\max}$: maximum $\dot{x}_0$ that C satisfy 100-step convergence condition for $IC = [\dot{x}_0, 90, 0]$.
- $\Delta\varphi_{\max}$: maximum $\Delta\varphi_0 = |\varphi_0 - 90^\circ|$ that the controller is able to reduce to less than $\Delta\varphi_0/10$ in 100 steps and satisfy 100-step convergence condition for $IC = [0, \varphi_0, 0]$.
- $\Delta\dot{\varphi}_{\max}$: maximum $\dot{\varphi}_{t0}$ that the controller is able to reduce to less than 5 deg s^{-1} in 100 steps and satisfy 100-step convergence condition for $IC = [0, 90, \dot{\varphi}_0]$.

Based on these definitions, the controller with the most robust hopping is the one with the largest values for tolerable perturbations. The target investigates the effect of different parameters such as leg mass, damping, μ and stiffness on the robustness of the controllers. The maximum perturbations $\Delta\dot{x}_{\max}$, $\Delta\varphi_{\max}$ and $\Delta\dot{\varphi}_{\max}$ are limited to 6 m s^{-1}, 90 deg and 230 deg s^{-1}, respectively. These limits are far beyond the maximum perturbation applied in human experiments from which the subjects could recover in few steps. Such high limits show the ability of the control method in more difficult situations.

3. Results

In this section, the ability of the proposed control system to induce stable and robust hopping motion is investigated. We start with the TSLIP model and show the results, first for VPPC-FP and then for VPPC-LQR. We apply the same approach to the XTSLIP, for which we additionally compare the results for the aVPPC and the eVPPC, both with event-based control. The influences of the model parameters (leg mass m_l and dimensionless leg damping $\tilde{d}$) are also investigated.

3.1. TSLIP model

3.1.1. VPPC with fixed VPP position (VPPC-FP). First, the parameters' space is explored to find the stable hopping motions with the nominal hopping height ($y_d = 1.125$ m). For the controller, the variable parameters are μ and r_{VPP}, as γ is fixed to zero with VPPC-FP. We also consider the influence of the leg stiffness on stability, a model parameter that could be adjusted to improve the hopping performance.

As explained in section 2.2.2, the stability of a periodic hopping motion is investigated using Poincarre map analysis and characterized using the λ_{Max}, the magnitude of the largest eigenvalue of the Jacobian matrix of the mapping function. Figure 4 (left) represents a map of the value of λ_{Max} in the considered parameter space. It shows that, for all three stiffness values, there exists large parameter regions resulting in stable hopping (however the eigenvalues are close to one). For all further analyses with the TSLIP and XTSLIP models, we choose the intermediate value $\tilde{k} = 20$.

Next, the robustness of the hopping motions against perturbation is evaluated. The results are represented in figure 5, for different values of the controller parameters. It shows that the system, in addition to being stable, can also be highly robust against perturbations, but only in a limited range of parameters. In particular, moving the VPP point away from the CoM (larger r_{VPP}) appears to improve the performance, both with respect to stability and robustness.

Although these results show that the controller is able to stabilize the system and handle large perturbations, disturbance rejection with VPPC-FP is generally slow. This could be expected from the values of λ_{Max} which are close to 1, as shown in figures 4 and 5. This situation is illustrated in figure 6, depicting the system response after simultaneous perturbations of $\dot{x}$, φ and $\dot{\varphi}$. Even for parameter values with the smallest value of λ_{Max} found in figure 5 ($r_{\text{VPP}} = 0.08$ m and $\mu = 0.36$), more than 95 s are needed to reject 95% of the perturbation on φ. This is the settling time for the time response.

3.1.2. VPPC with event-based control (VPPC-LQR). As explained in section 2.3.3, event-based control of the VPP position (using γ) allows us to improve the system behavior by placing the poles of the close loop system matrix $A - BK$ in desired positions. The only necessary condition is the controllability of the pair $[A, B]$, which is always satisfied for this problem. In addition, using discrete LQR for the selection of the gain vector K, we can use the weight matrix W in equation (11) to give more importance to some of the state variables. For our simulation, we set $W = \text{diag}[8, 1, 1]$, hence giving a higher importance to the trunk angle which is the main control target.

Using VPPC-LQR, periodic hopping motions with nominal hopping height can be stabilized everywhere in the parameter space previously considered in figure 4. Comparing figure 7 to figure 5 reveals that lower eigenvalue λ_{Max} are achieved with this approach. Figure 7 also shows that very high robustness against perturbations is achieved. In addition, VPPC-LQR is much more robust against parameter variations,

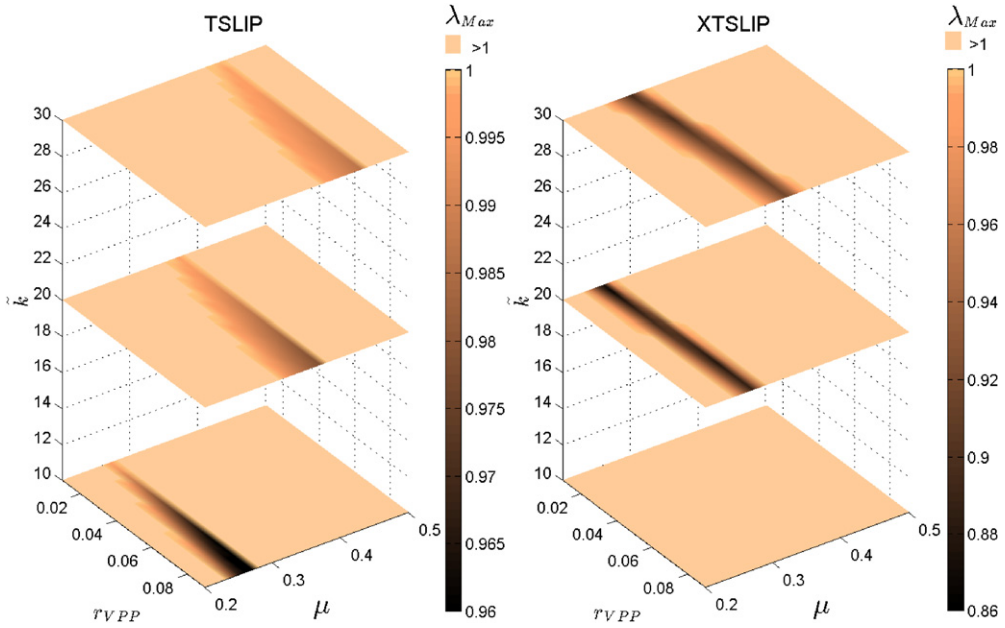

Figure 4. The largest eigenvalues' magnitude λ_{Max} of the VPPC-FP controller for ranges of the controller parameters (μ and r_{VPP}) and the leg stiffness ($\tilde{k}$). In TSLIP, for the stable controllers, λ_{Max} is very close to 1. In XTSLIP ($\tilde{d} = 0$), stable responses have eigenvalues smaller than TSLIP, but no stability exists for $\tilde{k} = 10$, ($\lambda_{\text{Max}} > 1$).

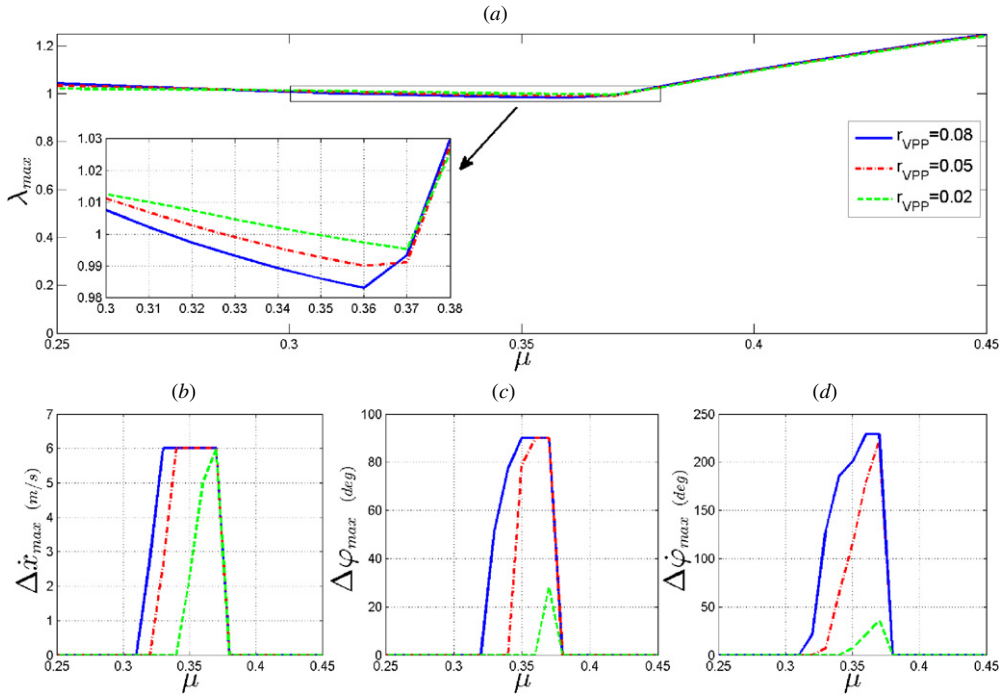

Figure 5. (*a*) Stability and ((*b*), (*c*) and (*d*)) robustness against perturbations for the TSLIP with VPPC-FP controller, with respect to controller parameters μ and r_{VPP} ($\tilde{k} = 20$).

as the performances are much less dependent on the parameter values (r_{VPP} and μ) as for VPPC-FP. This is likely related to the fact that LQR is a robust controller against the model uncertainties [31].

Finally, the improvements regarding disturbance rejection are illustrated in figure 6, where the response of the system after perturbation is shown for VPPC-FP and VPPC-LQR. For VPPC-LQR, the results for two sets of parameter values are presented. First, the same parameter set as for VPPC-FP (i.e. $\mu = 0.36$) were considered for the sake of comparison. The results show already a considerable improvement of the response, with respect to the disturbance rejection rate. The required time to decrease the trunk deviation and horizontal velocity to less than 5% of their initial values is about 7.5 s. This time is even less for $\dot{\varphi}$. For the second parameter set, we used the values found in figure 7 to result in the smallest λ_{Max}

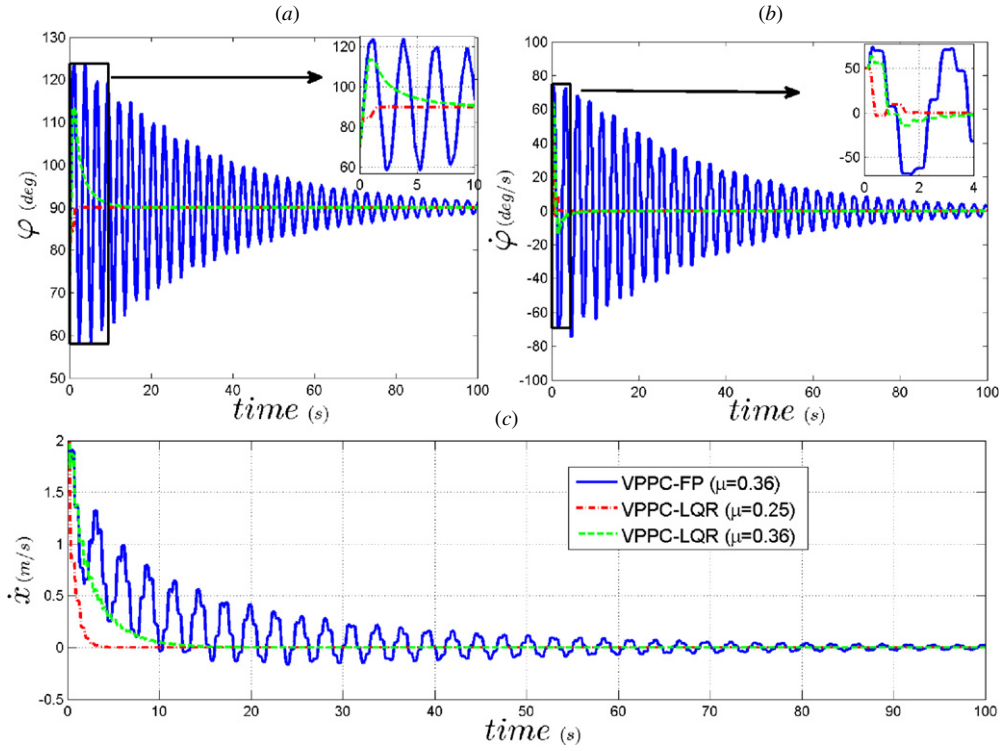

Figure 6. The trunk (*a*) angle, (*b*) angular velocity and (*c*) horizontal velocity responses of the system to perturbations for the TSLIP model with VPPC-FP and VPPC-LQR. The perturbations result in $[\dot{x}_0, \Delta\varphi_0, \dot{\varphi}_0] = [2\,\mathrm{m\,s^{-1}}, 20\,\mathrm{deg}, 50\,\mathrm{deg\,s^{-1}}]$ and $r_{\mathrm{VPP}} = 0.08\,\mathrm{m}$.

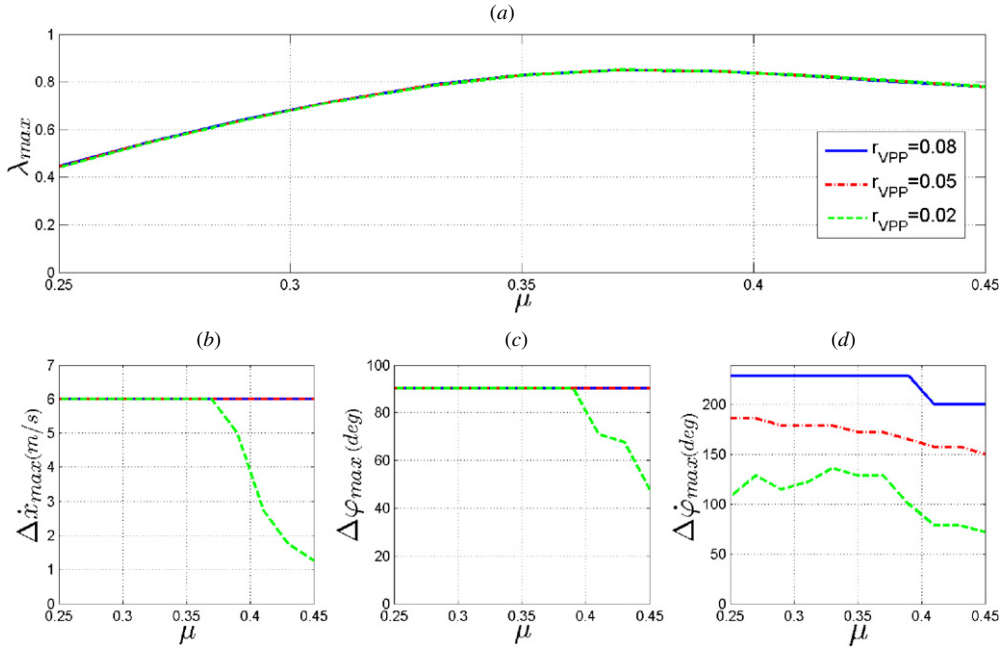

Figure 7. (*a*) Stability and ((*b*), (*c*) and (*d*)) robustness against perturbations for the TSLIP model with VPPC-LQR controller, with respect to the controller parameters μ and r_{VPP}.

(i.e. $\mu = 0.25$). As expected, the performances were further improved, with 95% rejection achieved in less than 2 s. In comparison with VPPC-FP, reduction of the settling time to 8% and 2% was achieved with the first and second parameter sets, respectively. These results show that introducing event-based adjustment of γ not only improves the stability, but also allows for fast disturbance rejection and high robustness with respect to perturbation and parameter variations.

3.1.3. Comparison of VPPC–LQR with HZD controller. To investigate the quality of the proposed approach, we implemented HZD (Hybrid Zero Dynamics) control method

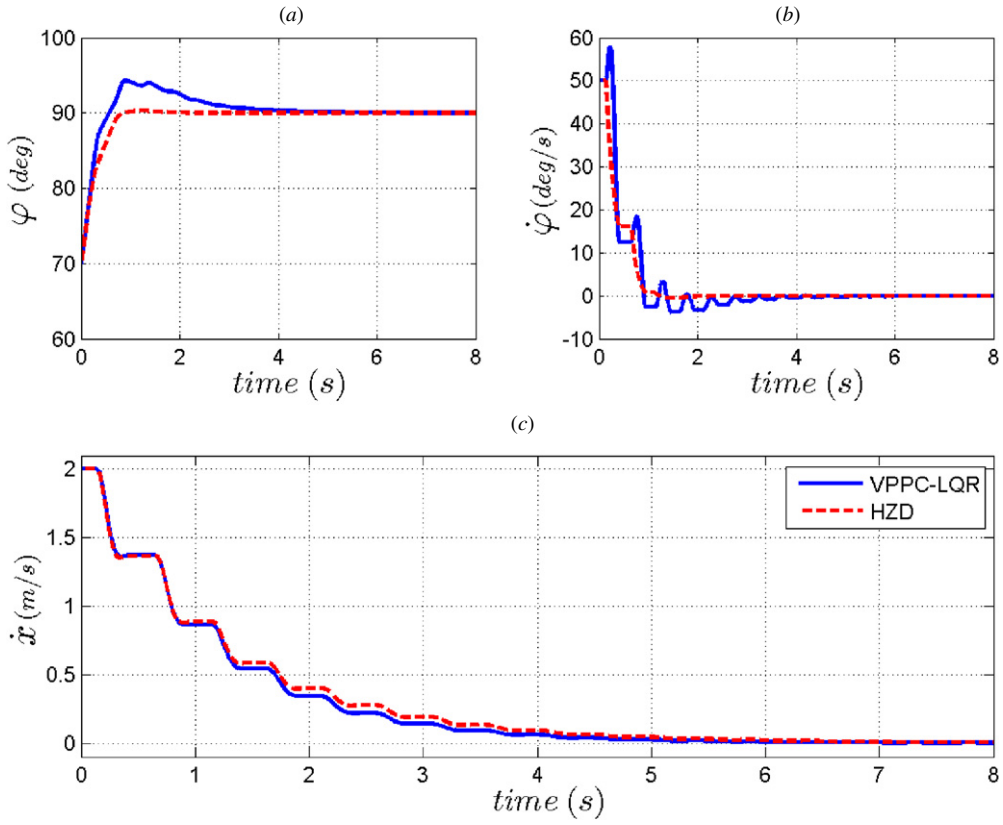

Figure 8. Comparison between VPPC-LQR and HZD for trunk stabilization for TSLIP model. The perturbations result in $[\dot{x}_0, \Delta\varphi_0, \dot{\varphi}_0] = [2\ \mathrm{m\,s^{-1}}, 20\,\mathrm{deg}, 50\,\mathrm{deg\,s^{-1}}]$.

for hip torque as an alternative [32]. Using this method, the difference of the trunk angle from upright position is considered as the output which should become zero. This is done by feedback linearization which reduces the stability problem of the complete system to analyzing the stability of the zero dynamics. With precise measurement and knowing the exact model, HZD could have the highest tracking performance with exponentially stable properties. Thus, it is considered as a reference for assessing the performance of the method. The quality of HZD control compared with VPPC-LQR is shown in figure 8. It is observed that convergence to upright position and zeroing the trunk angular speed is faster than VPPC-LQR with less oscillations, but the horizontal velocity becomes zero slightly slower. General behaviors of these two methods are comparable, but the HZD controller is more complex and needs a precise model and more sensory information.

3.2. XTSLIP

In this section, stability, robustness and disturbance rejection performances of the proposed approaches are presented for the XTSLIP model. The main difference between this model and the TSLIP model is the relaxation of the simplifying modeling assumption that the mass of the leg can be neglected. For this reason, we first investigate shortly how the introduction of mass in the leg influences the stability behavior.

3.2.1. Influence of the leg mass. To investigate this point, we considered a series of intermediate models, with the leg mass and leg inertia increasing from zero, as in the TSLIP model, to their values in the XTSLIP model. The mass and the CoM position of the trunk were adapted in order to keep constant the total mass and CoM position when standing. For each model, we investigated the stability and the robustness.

The results of this investigation are presented in figure 9 for VPPC-LQR (note that we found the same tendencies for VPPC-FP). The controller parameters μ and r_{VPP} were kept constant to allow for fair comparison between the models. On the one hand, increasing leg mass ratio ($p = \frac{m_l}{m}$) results in the degradation of the robustness against perturbation. This was to be expected because the increase of the leg mass, combined with the saturation of the hip torque, limits the speed of the leg adjustment and consequently impacts the action of the VBLA. In addition, the action of the VBLA during the swing phase produces a counteracting torque on the trunk. This increases in turn the perturbation of the trunk orientation that the VPPC must deal with. On the other hand, figure 9 shows a small but consistent improvement of the stability.

3.2.2. VPPC with fixed VPP position (VPPC-FP). Because of two aforementioned reasons the stability region is smaller after the addition of mass to the leg in figure 4 (right). For $\tilde{k} = 10$, no stable region at all is found in the whole range investigated for μ and r_{VPP}. Nevertheless, comparing this figure with figure 4 (left) shows that for stable regions, in XTSLIP the eigenvalues are less than in TSLIP. This is reflected by the eigenvalues shown for $\tilde{k} = 20$ and $r_{\mathrm{VPP}} = 0.05$ in figure 10. The robustness against perturbations is less than

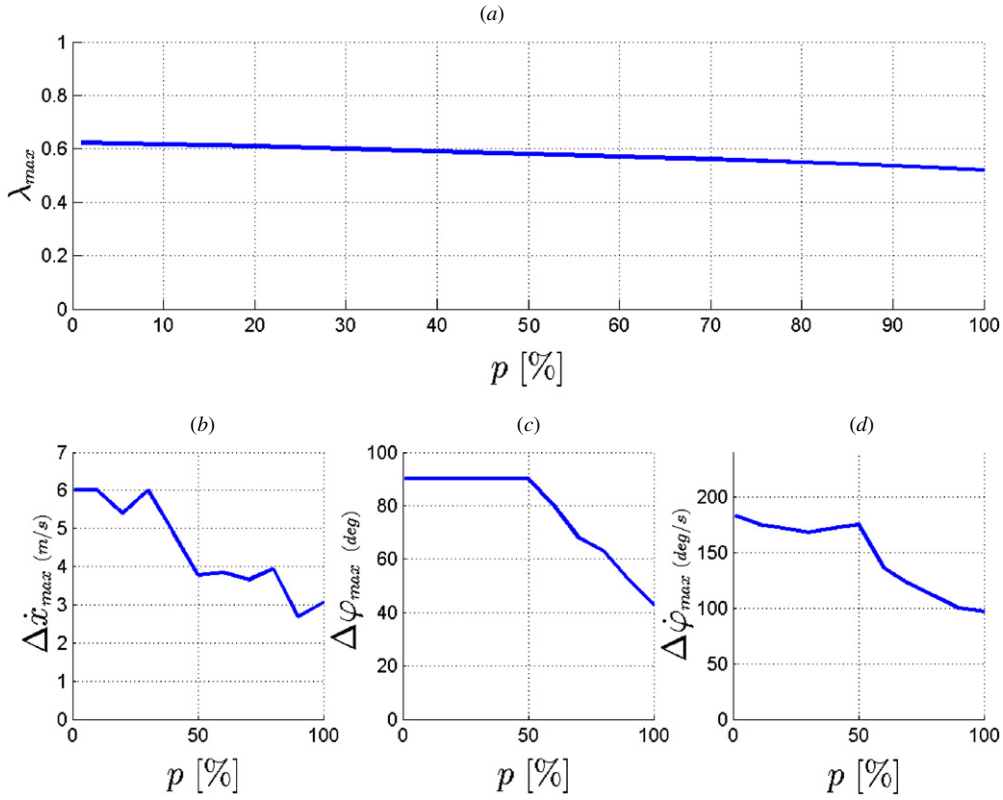

Figure 9. Influence of the leg mass/inertia ratio (p) on (a) the stability and (b), (c) and (d) robustness against perturbations for VPPC-LQR. ($\mu = 0.29$, $\tilde{d} = 0$ and $r_{\mathrm{VPP}} = 0.05$).

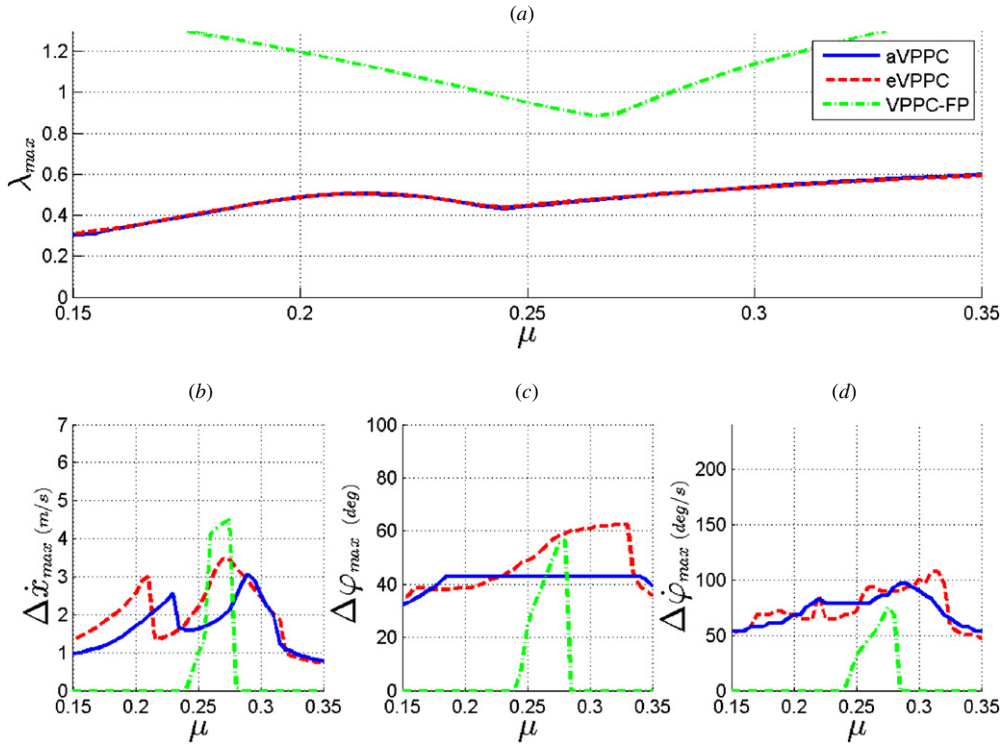

Figure 10. (a) Stability and ((b), (c) and (d)) robustness against perturbations for the XTSLIP model w.r.t the control parameter μ. ($\tilde{k} = 20$, $r_{\mathrm{VPP}} = 0.05$ and $\tilde{d} = 0$).

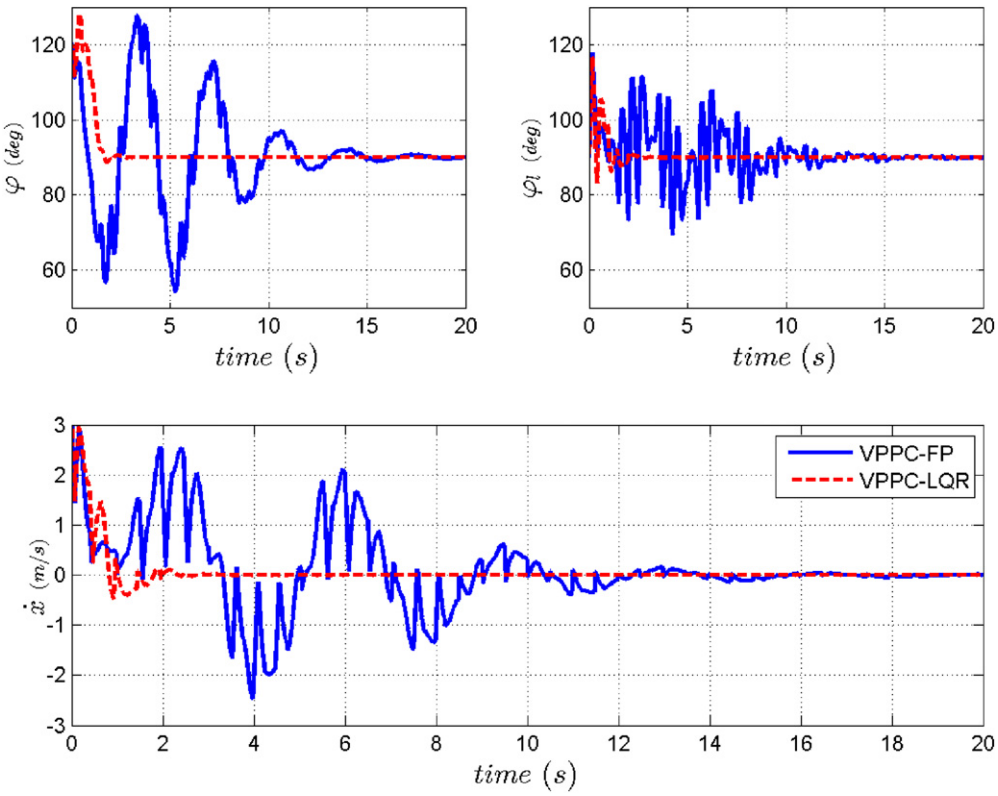

Figure 11. Comparison of (*a*) trunk angle, (*b*) leg angle and (*c*) horizontal velocity between VPPC-FP and VPPC-LQR in time domain. The perturbations result in $[\dot{x}_0, \Delta\varphi_0, \dot{\varphi}_0] = [3\ \mathrm{m\,s^{-1}}, 30\ \mathrm{deg}, 50\ \mathrm{deg\,s^{-1}}]$. For VPPC-FP and VPPC-LQR, μ is equal to 0.27 and 0.29, respectively and $\tilde{d} = 0.1$.

that in TSLIP controlled by VPPC-FP, but it is considerable. The best performance (the lowest eigenvalue and the largest tolerable perturbations) is achieved for $\mu = 0.27$. Similar trends (with minor changes) are observed when damping is nonzero. The time responses for the horizontal velocity, and the leg and trunk angles are displayed in figure 11 when the damping ratio is 10% ($\tilde{d} = 0.1$). It is shown that all the perturbations are removed within 15 s. It is predicted that with mass and inertia in the leg, convergence to stable vertical hopping is faster. The observed oscillations resulted from applied torque for leg adjustment during the flight phase.

3.2.3. VPPC with LQR (VPPC-LQR). To emphasize the significance of trunk angle the weights are selected as $W = \mathrm{diag}[0, 8, 1, 0, 1]$ like in TSLIP. Similar to the TSLIP model, using VPPC-LQR guarantees stability in the whole considered parameter domain. Figure 11 shows better performance of VPPC-LQR with respect to the original VPPC-FP. It removes all perturbations in only 2 s. The aVPPC as the simplified version of the proposed controller VPPC-LQR is perfect in diminishing perturbations.

In order to investigate the effect of this simplification, the robustness of aVPPC and eVPPC was compared (see figure 10). In this section, the robustness of the controlled motion against perturbations is evaluated for different system parameters. It is shown that aVPPC has the same eigenvalues and similar robustness as the exact controller for XTSLIP. In spite of robustness reduction compared with the TSLIP model, it is sufficient for perturbed hopping. To find the best compromise between robustness and fast convergence to periodic motion, we selected $\mu = 0.29$ for evaluation in time domain (see figure 11). For this value, the perturbations exerted in figure 11 are near their maximum tolerable ones. It shows that the controller works well when all perturbations happen together and mass and damping exist in the leg (figure 1(*b*)).

Finally, damping effects on control are evaluated when the other parameters are fixed and μ is optimized for the model without damping[5]. The results are displayed in figure 12. It shows that the eigenvalues are mostly increased with increasing the damping. So the convergence becomes slightly slower with higher damping. For horizontal velocity perturbations (figure 12(*a*)), the robustness reduces with damping, whereas for the trunk angle and angular velocity (figures 12(*c*) and (*d*)), the effect of damping on robustness is less monotonic. It is not significant and the system is sufficiently robust against perturbations even with high damping coefficients. In all the results for robustness and eigenvalues, strict implementation of VPPC only results in a slight increase of the robustness. Hence, the approximate implementation of VPPC is efficient, especially because it requires less sensory information.

[5] With other values (e.g. $\mu = 0.26$ which gives the minimum eigenvalue for $\tilde{d} = 0.1$) minor differences are observed in the results.

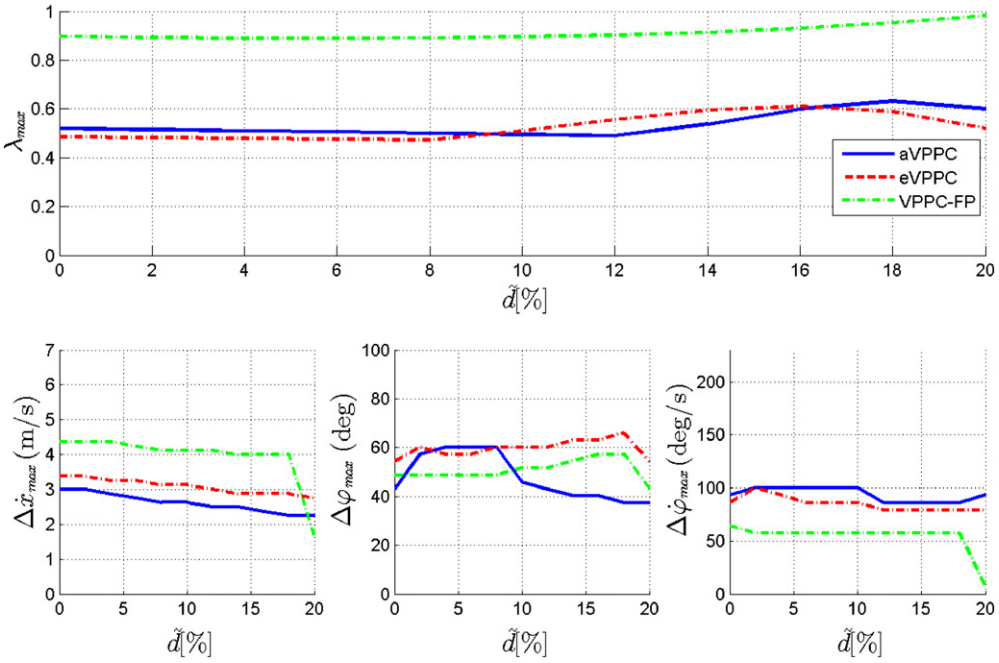

Figure 12. Comparison between aVPPC, eVPPC and VPPC-FP with respect to (*a*) stability and (*b*), (*c*) and (*d*) robustness against different perturbations dependent on the damping coefficient ($\tilde{d}$) for XTSLIP model. The normalized damping ratio values are presented in percent, e.g. 10% means $\tilde{d} = 0.1$. ($\mu = 0.27$ and $r_{\text{VPP}} = 0.05$).

4. Discussion

Hopping is a fundamental requirement for running in two basic functions: bouncing and balancing. In addition, for robust hopping against perturbations, swinging the leg in the flight phase is observed. Three different approaches are presented to perform robust hopping. First, leg length adjustment is applied for stable bouncing with a nominal hopping height. Second, VPPC is utilized for balancing that tries to keep the trunk in upright position. Finally, VBLA is the proposed technique for swing leg adjustment.

For the SLIP model, VBLA and hopping height control are able to remove any perturbations at most in two steps. A comparison between VBLA, Peuker's and Raibert's approach with respect to human leg adjustment in perturbed hopping was presented recently [33]. Among these approaches, VBLA showed the most robust behavior with fewest required parameters. In the SLIP model extended with trunk, leg mass and damping, balancing turns out to be the most significant task.

It is remarkable that VPPC-FP (with fixed VPP) could create stable hopping with upright trunk without measuring the trunk orientation. However, it is very slow in disturbance rejection and not very robust against parameter changes. Adaptation of the VPP position via event-based control not only results in faster convergence to periodic vertical hopping (because of smaller eigenvalues), but also increases the robustness against perturbations and uncertainties. With this approach, it is possible to achieve stable hopping in the whole investigated parameter region, because stability is guarantied by the controller design. This gives the freedom to select the value of the model parameters, such as the leg stiffness, to reach other objectives, including minimizing energy consumption or satisfying constraints on the maximal torque.

Different approaches to adjust the VPP point using feedback control were investigated in [13]. Amongst them, LQR as an optimal control approach offered the best trade-off between convergence rate and reduction of the response overshoot. In addition, this method offers the possibility of adjusting the controller behavior with the weight matrix W, in order to prioritize disturbance rejection for a specific system state. Regarding sensory information, the only cost for all these benefits is to measure or estimate the system state at apex. Event-based control also requires a linear map of the apex-to-apex behavior of the model, around a desired hopping motion, but it can be computed offline and once for each nominal hopping condition.

Adding mass and damping to the leg makes the model more realistic and influences the performance of all control layers. Large hip torques may be needed to track the desired leg angle in the flight phase and disturb the trunk orientation which needs to be compensated during the stance phase. Another consequence is that the equation governing the hip torque, required to redirect exactly the GRF towards the VPP, becomes much more complex and requires the knowledge of the system state during the stance phase. However, we found out that using the simpler relation, previously employed for the TSLIP model, and which is only an approximation for the XTSLIP model, leads to the comparable results as the exact one. Therefore, we could keep both the simplicity and quality of the control approach with the more complex model.

HZD is another control approach utilized to keep the trunk upright (instead of VPPC) in hopping and running with TSLIP model [34]. Although this method results in very small eigenvalues and fast convergence rate, it requires a precise

model of the system and the knowledge of the system state during the stance phase. Hence, for more complicated models (such as the XTSLIP), it results in an increased complexity of the controller, while this was not so critical in our approach (using aVPPC). In addition, VPPC-LQR can produce similar performance with lower complexity and less required sensory information. Therefore, with respect to other control methods, the main benefit of our approach is the ability to achieve robust behavior with limited efforts, in terms of parameter tuning, model accuracy and sensory feedback.

The proposed controller was able to reject very large perturbations, such as changes in the horizontal speed by 3 m s^{-1}, in the trunk angle by 50° and in the angular velocity by 80 deg s^{-1}. This holds even if all these changes happen simultaneously (figure 11). High robustness against variations of damping, leg mass and even the control parameters for VBLA support the application of the controller in practice.

The VPP concept was shown to be relevant not only in human locomotion but also for animals (e.g. bird running). This demonstrates that the underlying mechanical concept may be applied to different body morphologies or robot designs. Preliminary simulation results for a model corresponding to the specific robot design show that this controller is robust and easy to adapt. There are several potential extensions of this control approach. One extension would be to apply it to a model with segmented legs. Then, the posture control will not just be realized at a single joint level (e.g. hip joint). In order to employ similar control schemes as presented in this paper, it would be required to map the joint space of the segmented leg to the virtual leg axis as described by the XTSLIP model. There are many approaches to produce this projection, such as virtual model control [35] or SLIP-embedding approach [7]. Another option can be using a set of differentials to create a virtual prismatic leg between the hip and the toe to control the virtual leg (length and angle) with respect to the trunk via different actuators [18].

Appendix A. Derivation of the equations of motion for the XTSLIP model

We derive the equations of motion of the system by using an approach, sometimes called the TMT method, that yields equations equivalent to the Lagrange equations but with the system matrices in a factorized form. This facilitates the fast numerical simulation of the system. The equations of motion when the system is in the flight phase can then be written as follows:

$$T^T M T \ddot{q} + T^T M D = T^T [G + H + \Gamma] \tag{A.1}$$

with

$$q = [x, y, \varphi_l, \varphi]^T \tag{A.2}$$

$$T = \begin{bmatrix} 1 & 0 & r_{\text{leg}} \sin\varphi_l & 0 \\ 0 & 1 & -r_{\text{leg}} \cos\varphi_l & 0 \\ 0 & 0 & 1 & 0 \\ 1 & 0 & 0 & -r_{\text{CoM}} \sin\varphi \\ 0 & 1 & 0 & r_{\text{CoM}} \cos\varphi \\ 0 & 0 & 0 & 1 \end{bmatrix};$$

$$D = \begin{bmatrix} r_{\text{leg}} \cos\varphi_l \, \dot{\varphi_l}^2 \\ r_{\text{leg}} \sin\varphi_l \, \dot{\varphi_l}^2 \\ 0 \\ -r_{\text{CoM}} \cos\varphi_t \, \dot{\varphi}^2 \\ -r_{\text{CoM}} \sin\varphi_t \, \dot{\varphi}^2 \\ 0 \end{bmatrix} \tag{A.3}$$

$$M = \text{diag}([m_l, \ m_l, \ J_l, \ m_t, \ m_t, \ J_t]);$$
$$G = -g.[0 \ , \ m_l \ , \ 0 \ , \ 0 \ , \ m_t \ , \ 0]^T \tag{A.4}$$

$$H = [F_{\text{leg}} \cos\varphi_l, \ F_{\text{leg}} \sin\varphi_l, \ 0, \ 0, \ 0, \ 0]^T;$$
$$\Gamma = [0, \ 0, \ \tau, \ 0, \ 0, \ -\tau]^T, \tag{A.5}$$

where x, y, φ_l, φ and F_{leg} are respectively the horizontal and vertical positions of the hip, the orientations of the leg and the trunk and the leg force. The other symbols refer to parameters that were defined in table 1.

During the stance phase, the contact of the foot with the ground constrains the motion of the system. This is achieved by using the Lagrange multiplier approach, hence, by introducing an explicit constraint force in the equations of motion and appending the additional equation describing the constraint. In this case, the constraint force is essentially the ground reaction force applied in the direction perpendicular to the leg axis (as the leg is free to compress along the leg axis, due to the presence of the spring). Using the notations $A = T^T M T$ and $B = T^T [MD - G - H]$, the constrained equations of motion are written as

$$\begin{cases} A\ddot{q} + B = T^T \Gamma + J^T F_N \\ J\ddot{q} + C = 0 \end{cases} \tag{A.6}$$

with

$$J = [\sin\varphi_l, \ -\cos\varphi_l, \ \sin(\varphi_l) \ (y - y_f) + \cos\varphi_l \ (x - x_f), \ 0] \tag{A.7}$$

$$C = 2 \, \dot{\varphi_l} \, \dot{x} \, \cos\varphi_l + 2 \, \dot{\varphi_l} \, \dot{y} \, \sin\varphi_l - \dot{\varphi_l}^2 \, y_f \, \cos\varphi_l + \dot{\varphi_l}^2 \, y \, \cos\varphi_l + \dot{\varphi_l}^2 \, x_f \sin\varphi_l - \dot{\varphi_l}^2 \, x \, \sin\varphi_l, \tag{A.8}$$

where x_f and y_f are respectively the horizontal and vertical positions of the contact point of the foot with the ground and F_N is the component of the GRF perpendicular to the leg axis.

Appendix B. Derivation of the eVPPC equations for the XTSLIP model

To implement the eVPPC approach, we want to compute the hip torque τ that will produce the desired F_N that will redirect the GRF vector towards the VPP. After the manipulation of equation (A.6), we have

$$E\Gamma = -C + JA^{-1}B - JA^{-1}J^T F_N \tag{B.1}$$

with $E = JA^{-1}T^T$. As E is a vector and given the form of Γ, the hip torque τ for eVPPC with the XTSLIP model is given by

$$\tau = (-C + JA^{-1}B - JA^{-1}J^T F_N)/(E(3) - E(6)) \tag{B.2}$$

Appendix C. Derivation of hopping height control equations

The leg rest length is adjusted at maximum leg compression point; then, we initiate the motion from this moment ($t = 0$). The target is finding desired leg rest length that the vertical hopper with compressed length y_c reaches the desired height y_d at the next apex. Then, the border conditions to solve the motion equation versus time at stance phase will be as follows:

$$\begin{cases} y(0) = y_c \\ \dot{y}(0) = 0 \end{cases} \quad \text{initial conditions}$$
$$\begin{cases} y(t_{to}) = l_d - \mathrm{d}v_{to}/k \\ \dot{y}(t_{to}) = v_{to} \end{cases} \quad \text{take off conditions,} \tag{C.1}$$

where t_{to} and v_{to} are the time and velocity at TO (when the leg reaches its rest length with positive velocity), respectively. According to conservative (ballistic) motion in the flight phase, equality of energy at TO and apex results in

$$\tfrac{1}{2}mv_{to}^2 = mg(y_d - l_d + \mathrm{d}v_{to}/k) \Rightarrow v_{to} = s + \sqrt{s^2 + 2g(y_d - l_d)} \tag{C.2}$$

For $d^2 < 4$ km, the response of the differential equation (15) is obtained as

$$y(t) = \mathrm{e}^{-\beta\omega t}(\alpha_1 \sin(\omega t) + \alpha_2 \cos(\omega t)) + l_d - \frac{mg}{k}, \tag{C.3}$$

where α_1 and α_2 are computed using the initial conditions at $t = 0$ by the following relations:

$$\begin{cases} \alpha_2 = y_c - l_d + \dfrac{mg}{k} \\ \alpha_1 = \beta\alpha_2 \end{cases} \tag{C.4}$$

otherwise, it never reaches the rest length and the mass stops where the weight is equal to the spring force. From the border conditions at TO, two relations are obtained for l_d and t_{to}:

$$\begin{cases} \frac{mg - \mathrm{d}v_{to}}{k} = \mathrm{e}^{-\beta\omega t_{to}}(\alpha_1 \sin(\omega t_{to}) + \alpha_2 \cos(\omega t_{to})) \\ v_{to} = \omega\, \mathrm{e}^{-\beta\omega t_{to}}(-(\alpha_1\beta + \alpha_2)\sin(\omega t_{to}) \\ \qquad + (\alpha_1 - \alpha_2\beta)\cos(\omega t_{to})). \end{cases} \tag{C.5}$$

Defining $a = \frac{mg - \mathrm{d}v_{to}}{k}$ and using the relation between α_1 and α_2 in (C.4) with some manipulations, (C.5) results in

$$\begin{cases} \alpha_2 = \dfrac{a\, \mathrm{e}^{\beta\omega t_{to}}}{\beta \sin(\omega t_{to}) + \cos(\omega t_{to})} \\ v_{to} = \alpha_2 \omega\, \mathrm{e}^{-\beta\omega t_{to}}(\beta \sin(\omega t_{to}) - a\beta\omega); \end{cases} \tag{C.6}$$

then,

$$\overbrace{\beta + \frac{v_{to}}{a\omega}}^{P_{l_d}} = \frac{\beta\cos(\omega t_{to}) - \sin(\omega t_{to})}{\beta \sin(\omega t_{to}) + \cos(\omega t_{to})}. \tag{C.7}$$

Let $\gamma = \arcsin\left(\frac{\beta}{\sqrt{1+\beta^2}}\right)$, which results in $t_{to} = \frac{\gamma - \arctan(P_{l_d})}{\omega}$. Putting t_{to} in (C.6) gives

$$\alpha_2 = a \exp(\beta(\gamma - \arctan(P_{l_d})))\sqrt{\frac{1 + P_{l_d}^2}{1 + \beta^2}}. \tag{C.8}$$

Finally, from (C.4) which give $l_d = y_c + \frac{mg}{k} - \alpha_2$, the desired values for the leg length is

$$l_d = y_c + \frac{mg}{k} - a\sqrt{\frac{1 + P_{l_d}^2}{1 + \beta^2}} \exp(\beta(\gamma - \arctan(P_{l_d})). \tag{C.9}$$

References

[1] Full R J and Koditschek D 1999 Templates and anchors: neuromechanical hypotheses of legged locomotion on land *J. Exp. Biol.* **202** 3325–32

[2] Blickhan R 1989 The spring-mass model for running and hopping *J. Biomech.* **22** 1217–27

[3] McMahon T and Cheng G 1990 The mechanics of running: How does stiffness couple with speed? *J. Biomech.* **23** 65–78

[4] Geyer H, Seyfarth A and Blickhan R 2006 Compliant leg behaviour explains basic dynamics of walking and running *Proc. R. Soc.* **273** 2861–7

[5] Raibert M H 1986 *Legged Robots that Balance* (Cambridge, MA: MIT Press)

[6] Saranlı U, Buehler M and Koditschek D 2001 Rhex: a simple and highly mobile robot *Int. J. Robot. Res.* **20** 616–31

[7] Poulakakis I and Grizzle J W 2009 The spring loaded inverted pendulum as the hybrid zero dynamics of an asymmetric hopper *IEEE Trans. Autom. Control* **54** 1779–93

[8] Maus H M, Lipfert S, Gross M, Rummel J and Seyfarth A 2010 Upright human gait did not provide a major mechanical challenge for our ancestors *Nature Commun.* **1** 1–6

[9] Gruben K G and Boehm W L 2012 Force direction pattern stabilizes sagittal plane mechanics of human walking *Hum. Mov. Sci.* **31** 649–59

[10] Hyon S H and Emura T 2005 Symmetric walking control: Invariance and global stability *ICRA: IEEE Int. Conf. on Robotics and Automation* pp 1443–50

[11] Maus H M, Rummel J and Seyfarth A 2008 Stable upright walking and running using a simple pendulum based control scheme *CLAWAR: 11th Int. Conf. on Climbing and Walking Robots and the Support Technologies for Mobile Machines* pp 623–9

[12] Seyfarth A, Geyer H, Guenther M and Blickhan R 2002 A movement criterion for running *J. Biomech.* **35** 649–55

[13] Sharbafi M A, Maufroy C, Seyfarth A, Yazdanpanah M J and Ahmadabadi M N 2012 Controllers for robust hopping with upright trunk based on the virtual pendulum concept *IROS: IEEE/RSJ Int. Conf. on Intelligent Robots and Systems* pp 2222–7

[14] Maufroy C, Maus H M and Seyfarth A 2011 Simplified control of upright walking by exploring asymmetric gaits induced by leg damping *RoBio: IEEE Int. Conf. on Robotics and Biomimetics* pp 491–6

[15] Blickhan R and Full R J 1993 Similarity in multi-legged locomotion: Bouncing like a monopode *J. Comparative Physiol.* A **173** 509–17

[16] Altendorfer R, Moore N, Komsuoglu H, Buehler M, Brown H B, McMordie D, Saranli U, Full R D and Koditschek D E 2001 Rhex: a biologically inspired hexapod runner *Auton. Robots* **11** 207–13

[17] Ankaral M M and Saranli U 2010 Stride-to-stride energy regulation for robust self-stability of a torque-actuated dissipative spring-mass hopper *Chaos* **20** 033121

[18] Sreenath K, Park H, Poulakakis I and Grizzle J W 2011 A compliant hybrid zero dynamics controller for stable, efficient and fast bipedal walking on MABEL *Int. J. Robot. Res.* **30** 1170–93

[19] Grimes J A and Hurst J W 2012 The design of atrias 1.0 a unique monopod, hopping robot *CLAWAR: Int. Conf. on Climbing and Walking Robots* pp 548–54

[20] Poulakakis I and Grizzle J 2007 Formal embedding of the spring loaded inverted pendulum in an asymmetric hopper *Proc. European Control Conf.* pp 1779–93

[21] Winter D A 2005 *Biomechanics and Motor Control of Human Movement* 3rd edn (Hoboken, NJ: Wiley)

[22] Bertsekas D 2000 *Dynamic Programming & Optimal Control* (Belmont, MA: Athena Scientific)
[23] Sato A and Beuhler M 2004 A planar hopping robot with one actuator: design, simulation, and experimental results *IROS: IEEE/RSJ Int. Conf. on Intelligent Robots and Systems*
[24] Peuker F, Maufroy C and Seyfarth A 2012 Leg adjustment strategies for stable running in three dimensions *Bioinspir. Biomim.* **7** 036002
[25] Gunther M and Blickhan R 2002 Joint stiffness of the ankle and the knee in running *J. Biomech.* **35** 1459–74
[26] Yen J T and Chang Y-H 2010 Rate-dependent control strategies stabilize limb forces during human locomotion *J. R. Soc. Interface Eng.* **7** 801–10
[27] Riese S and Seyfarth A 2012 Stance leg control: variation of leg parameters supports stable hopping *Bioinspir. Biomim.* **7** 016006
[28] Schmitt J and Clark J 2009 Modeling posture-dependent leg actuation in sagittal plane locomotion *Bioinspir. Biomim.* **4** 046005
[29] Howley B and Cutkosky M 2009 Safe control of hopping in uneven terrain *J. Dyn. Syst. Meas. Control* **131** 011012
[30] Farley C and Morgenroth D 1999 Leg stiffness primarily depends on ankle stiffness during human hopping *J. Biomech.* **32** 267–73
[31] Zou K, Doyle J C and Glover K 1996 *Robust and Optimal Control* (Upper Saddle River, NJ: Prentice-Hall)
[32] Westervelt E R, Grizzle J W, Chevallereau C, Choi J H and Morris B 2007 *Feedback Control of Dynamic Bipedal Robot Locomotion* (London: Taylor and Francis)
[33] Sharbafi M A and Seyfarth A 2013 Human leg adjustment in perturbed hopping *AMAM: 6th Int. Symp. on Adaptive Motion of Animals and Machines*
[34] Sharbafi M A, Yazdanpanah M J, Ahmadabadi M N, Maufroy C and Seyfarth A 2012 Switching from hopping to running with HZD controller *Dynamic Walking Conf.*
[35] Pratt J E, Chew C M, Torres A, Dilworth P and Pratt G 2001 Virtual model control: An intuitive approach for bipedal locomotion *Int. J. Robot. Res.* **20** 129–43